PHYSICAL REVIEW LETTERS

Spin States in Graphene Quantum Dots

J. Güttinger,* T. Frey, C. Stampfer,† T. Ihn, and K. Ensslin

Solid State Physics Laboratory, ETH Zurich, 8093 Zurich, Switzerland
(Received 19 February 2010; published 7 September 2010)

We investigate ground and excited state transport through small ($d \approx 70$ nm) graphene quantum dots. The successive spin filling of orbital states is detected by measuring the difference between ground-state energies as a function of a magnetic field. For a magnetic field in-plane of the quantum dot the Zeeman splitting of spin states is measured. The results are compatible with a g factor of 2, and we detect a spin-filling sequence for a series of states which is reasonable given the strength of exchange interaction effects expected by comparing Coulomb interaction energy and kinetic energy of charge carriers in graphene.

Spin qubits in quantum dots [1] are interesting candidates for the implementation of future quantum information processing. Single spin preparation, manipulation, and readout has so far been demonstrated predominately in GaAs-based systems [2,3]. Spin coherence times in such systems are limited by hyperfine coupling and spin-orbit interactions. In graphene-based nanostructures, both limitations are expected to be significantly reduced in strength [4–7]. The electrostatic tunability of graphene quantum dots as well as the observation of excited states have been demonstrated recently [8–12]. The g factor in graphene has been measured via conductance fluctuations [13], but the general spin properties of confined electrons in graphene have remained elusive.

Here we present transport measurements on a graphene quantum dot as a function of magnetic field and analyze the evolution of Coulomb peaks and excited states in both perpendicular and parallel magnetic fields.

A scanning force microscope picture of the sample is shown as an inset in Fig. 1(a). The graphene quantum dot in the center is connected via tunneling constrictions to source (s) and drain (d) contacts. It is tunable by the back gate (bg) and several in-plane gate electrodes, including the plunger gate (pg). The fabrication of the sample is described in detail in Ref. [14]. All measurements were performed in a dilution refrigerator with a base temperature of 90 mK.

The source-drain conductance of the device measured over a large back gate voltage range is shown in Fig. 1(a). The region of suppressed conductance between 0 and 13 V (''transport gap'' [15]) separates the hole-transport regime at low V_{bg} from the electron transport regime at high V_{bg}. Coulomb-blockaded transport through the quantum dot is observed in this region at closer inspection. Regions A and B indicate the gate voltage ranges of the two measurement regimes investigated in this Letter. Previous measurements in region A [16] gave evidence for an electron-hole crossover in the Coulomb-blockaded quantum dot around $V_{\text{bg}} = 5.5$ V.

The same conductance resonances scanned with the back gate in region A (B) can also be investigated by keeping V_{bg} fixed at -0.9 V (-1.8 V) and sweeping the plunger gate voltage. [See top axis in Fig. 1(a) for the calculated plunger gate voltage at $V_{\text{bg}} = -0.9$ V (region A) corresponding to the measured back gate voltage.]
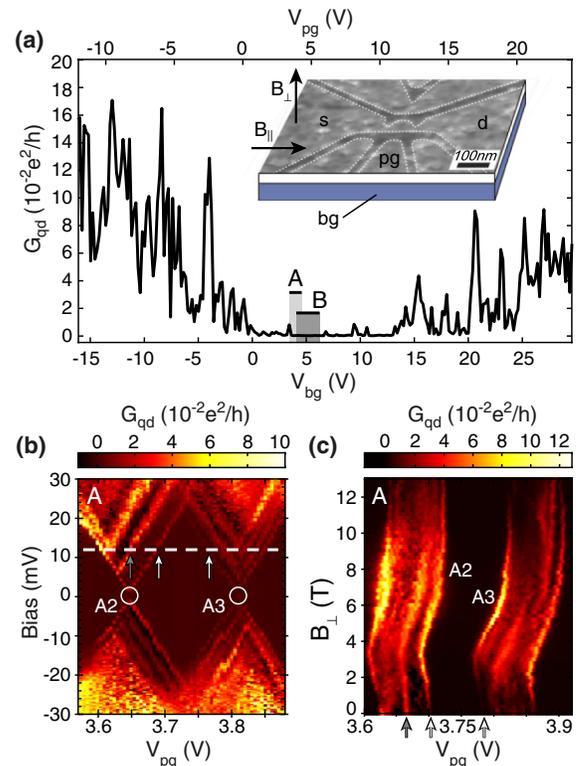
FIG. 1 (color online). (a) Quantum dot source-drain conductance for varying back gate voltage ($V_b = 100$ μV). (b) Coulomb diamond measurement recorded on the hole side of the electron-hole crossover. The gate dependence at $V_b = 11$ mV (white dashed line) for increasing perpendicular magnetic field is plotted in (c). Both edges of the diamond in (b) behave similarly in magnetic field, typical for spin pairs.

This plunger gate scale has been used throughout this Letter as a gate voltage scale to ease comparison.]

Two Coulomb-blockade resonances from regime A are investigated by measuring the differential conductance as a function of plunger gate voltage and source-drain bias at $B = 0$ T in Fig. 1(b). At $V_b = 0$ mV the differential conductance is suppressed except for the Coulomb resonance conditions (circles) where two conductance peaks $A2$ and $A3$ are observed. By increasing the bias window, a diamond-shaped region of blocked conductance is measured, revealing an electron addition energy of 20 meV. The change in differential conductance parallel to the edges of the diamond is attributed to excited states providing additional transport channels. Their energy splitting from the ground state is obtained directly from the measurement (e.g., 6 meV for the state marked with the gray arrow).

A cut through the diamond at $V_b = 11$ mV [dashed white line in Fig. 1(b)] for increasing magnetic field perpendicular to the graphene plane is shown in Fig. 1(c). After a kink around $B = 3.5$ T the edges of the diamonds move towards higher gate voltages with increasing field. This kink has been interpreted in Refs. [16,17] as an indication of filling factor two for holes in the quantum dot. The same kink is observed for the excited state resonance at $V_{\text{pg}} = 3.66$ V. The comparable evolution of the two diamond edges (white arrows) could be a result of spin pairing, i.e., two subsequently filled electrons occupying the same orbital state with opposite spin orientation.

Such pairs are interesting candidates for studying spin properties. In general, the extraction of a small Zeeman splitting from the magnetic field dispersion of individual conductance resonances is difficult, because any small orientational misalignment of the sample causes a significant $B_\perp$ component. Typically, the dispersion of states in the $B_\perp$ dominated by orbital effects is much stronger than the faint Zeeman splitting. Hence, small misalignment severely hampers the extraction of precise g-factor values from the dispersion of individual peaks. The problem can be circumvented by analyzing the peak-to-peak spacing of spin pairs, because orbital contributions can be significantly reduced by subtracting the positions of individual peaks sharing the same orbital shift [18,19].

Potential spin pairs are also identified in the gate regime B. In Fig. 2(a), the evolution of Coulomb peaks with increasing perpendicular field is displayed. The lowest two peaks ($B1$ and $B2$) and the following two ($B3$ and $B4$) are identified as potential spin pairs due to their similar peak evolution. In Fig. 2(b), a measurement of the same peaks is shown after careful *in situ* rotation of the sample into an orientation parallel to the magnetic field.

To analyze the movement of the peaks shown in Fig. 2, the peak positions are extracted by fitting. The results for the two pairs ($B1$–$B4$) in Fig. 2 and the pair ($A2$–$A3$) in Figs. 1(b) and 1(c) are shown in Fig. 3(a). Peak positions are plotted with suitable offsets in V_{pg} such that pairs
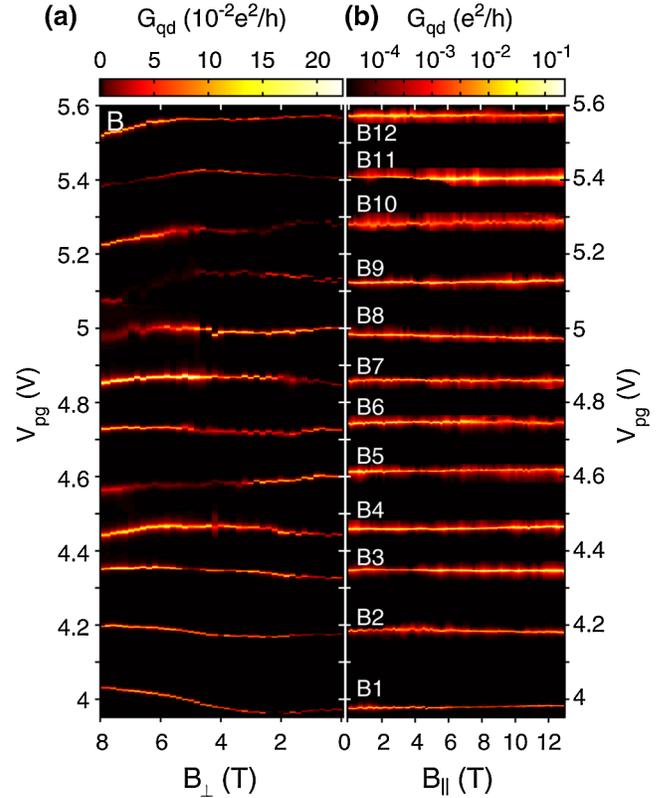
FIG. 2 (color online). (a) Coulomb peaks as a function of perpendicular magnetic field recorded at $V_b = 100 \ \mu$V. The conductance is plotted in linear scale to enhance visibility of amplitude changes. (b) The same Coulomb peaks measured in parallel (in-plane) magnetic field after tilting the sample by 90°. Here the conductance is plotted in logarithmic scale to increase the visibility of the peaks.

coincide at $B = 0$ T. For low $B_\perp$ ($B_\perp < 3$ T for $A2/A3$, $B1/B2$; $B_\perp < 6$ T for $B3/B4$), the orbital states of each pair have approximately the same B dependence. Hence spurious orbital contributions to the peak spacing resulting from slight misalignment are limited. The data in Fig. 3(a) for parallel orientation of the magnetic field show roughly linear splitting of pairs with increasing $B_\parallel$. We interpret this splitting as the Zeeman splitting of two spin states with identical orbital wave functions.

The magnitudes of the Zeeman splitting of the three pairs discussed above and two additional peak spacings are plotted in Fig. 3(b). The data are obtained in two steps. First, the peak-to-peak spacing from Fig. 2(b) and corresponding measurement in regime A is extracted. Second, the peak spacing is linearly fit from 4.2 to 13 T and the offset obtained from the fit is subtracted. The Zeeman spin splitting ΔE^Z is given by [19,20]

$$\Delta E^Z_{N+1} = (S_{N+1} - 2S_N + S_{N-1})g\mu_B B_\parallel + \text{const.}$$

Here S_N is the spin quantum number along the $B_\parallel$ direction of the dot with N electrons. Spin differences of successive ground states $\Delta S^{(1)}_{N+1} = S_{N+1} - S_N$ are half-integer
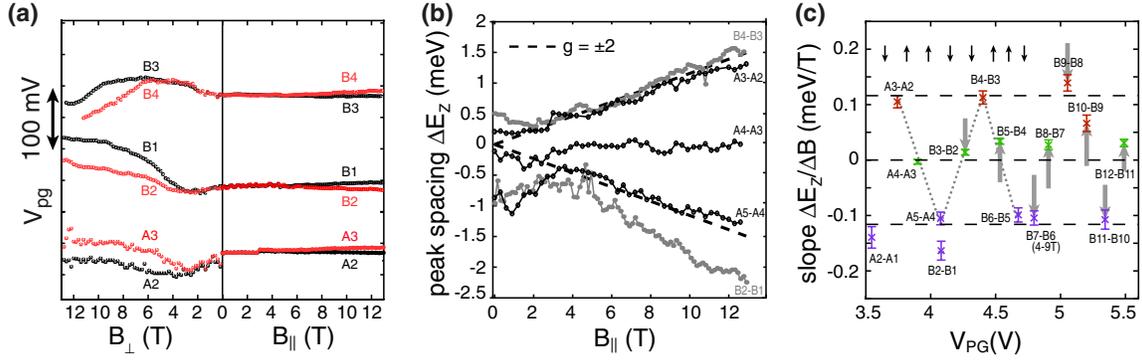
FIG. 3 (color online). (a) Comparing the evolution of three peak pairs in perpendicular (left) and parallel (right) magnetic field. (b) Coulomb peak spacing as a function of $B_\parallel$ for the three pairs shown in (a) and the two subsequent peak spacings (A4–A3 and A5–A4) in regime A. The dashed lines show the Zeeman splitting $\Delta E^z = \pm |g|\mu_B B$ for a g factor $|g| = 2$. All peaks are converted to energy by using the lever arm $\alpha_{pg} = 0.13 \pm 0.01$ as extracted from the corresponding Coulomb diamond measurements. (c) Slopes obtained by a linear fit for $B_\parallel = 4.2$–13 T of peak-to-peak spacings shown in (b) as a function of V_{pg}. The slopes of measurement B are compensated for by a parallel magnetic field misalignment of $\beta_B = 3°$ (see text), where the shift induced by the compensation is depicted by the gray arrows. The peak difference B7–B6 has a strong kink at $B_\parallel \approx 9$ T and is fitted only up to 9 T. The spin-filling sequence on top is extracted from the points along the dotted gray line.

values (e.g., $\Delta S^{(1)} = 1/2$ for adding a spin-up electron or $\Delta S^{(1)} = 3/2$ for adding a spin-up electron while "flipping" another spin from down to up). Hence differences between three successive spin ground states take on integer values $\Delta S_{N+1}^{(2)} = S_{N+1} - 2S_N + S_{N-1} = 0, \pm 1, \pm 2, \ldots$. Apart from the splitting of the pair B2–B1, the splitting of all pairs in Fig. 3(b) shows slopes $\Delta E^Z = \Delta S^{(2)} g\mu_B B_\parallel$ with integer values $\Delta S^{(2)} = 0, \pm 1$ and a g-factor value of approximately 2 [black dashed lines in Fig. 3(b)].

We now attempt to extract spin-related shifts from individual unpaired conductance resonances despite the inherent difficulty mentioned above. The final goal is to reconstruct a plausible spin-filling sequence of the quantum dot in regimes A and B. We apply the following strategy: First, the misalignment angle β is estimated, such that, second, the peak shifts in parallel field can be corrected for the orbital effects arising from the misalignment. Different angles β exist for measurements in regimes A and B, because the sample had been rotated into perpendicular orientation between the measurements B and A. The misalignment angle β was estimated by assuming $g = 2$ and linear peak shifts in $B_\perp$ in the range $0 \leq B_\perp \leq 2$ T and $B_\parallel$ in the range 4.2 T $\leq B_\parallel \leq$ 13 T. The angle β was then chosen to generate approximately $\Delta S_{N+1}^{(1)} = \pm 1/2$ for all peaks considered. The obtained values are $\beta_A = 0° \pm 0.5°$ and $\beta_B = 3° \pm 1°$. As a consequence, no correction for orbital effects was necessary in regime A.

The misalignment-compensated slopes of the peak spacings are shown in Fig. 3(c) as a function of V_{pg}. The gray arrows indicate the change of the slope by the compensation of the angular misalignment. The error bar includes the error from both the lever arm estimation (10% of the slope) and the variance from the linear fit of the peak-to-peak spacings. Three dashed black lines indicate the slopes corresponding to $\Delta E^Z / \Delta B = \{0, \pm 1\} \times 2 \ \mu_B$,

and the data points are colored according to their closest $\Delta S^{(2)}$ value (blue for $\Delta S^{(2)} = -1$, green for $\Delta S^{(2)} = 0$, and red for $\Delta S^{(2)} = +1$). Note that the two regimes A and B overlap: Pairs B2–B1 and A5–A4 are in fact the same Coulomb peaks as can be seen from a conductance measurement in dependence of V_{pg} and V_{bg} (not shown). We can extract the spin-filling sequence ↓↑↑↓↓↑↑↓ from peak A2 to B6 (dotted gray line). We emphasize that we see a clear deviation from ↑↓↑↓ as has been seen in the low carrier regime of carbon nanotube quantum dots [21–24].

This result can be made plausible by considering the exchange interaction between the charge carriers. The strength of the Coulomb interaction in graphene can be characterized by the ratio r_s between interaction energy and kinetic energy [25]:

$$r_s = \frac{E_{int}}{E_F} = \frac{e^2/(4\pi\epsilon_0\epsilon_r r_{ee})}{\sqrt{\pi\hbar^2 v_F^2 n_s}} = \alpha_g \approx 0.9,$$

independent of the charge carrier density n_s. Here $r_{ee} = (\pi n_s)^{-1/2}$ is the mean electron separation, v_F the Fermi velocity in graphene, and $\alpha_g = \alpha v_F/\epsilon_r c$ the *graphene fine-structure constant*. For the dielectric constant, a mixture of vacuum and SiO_2 $\epsilon_r = 2.5$ is used. The splitting of the eigenstate energies due to the exchange interaction can be estimated by using $\xi(r_s = 1) \approx 0.6\Delta$ [26–28]. The exchange energy splitting is comparable to the single-particle-level spacing Δ and can therefore lead to ground-state spin polarization $S > 1/2$ in agreement with our interpretation and observations in GaAs quantum dots [19,20]. An alternative reason for spin polarization in graphene could arise from the valley degeneracy. However, our measurements show no indications of fourfold shell filling as has been seen in carbon nanotubes [21,22,24].
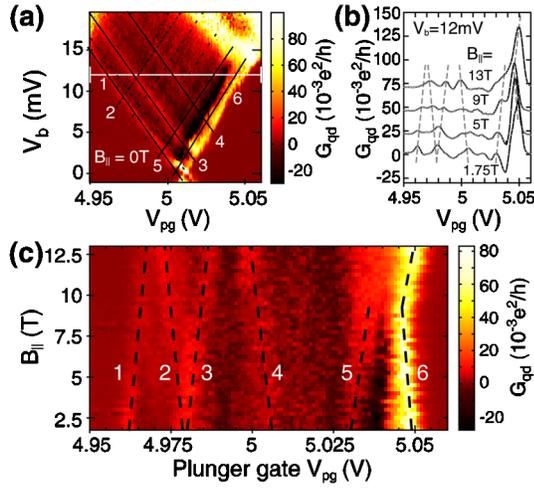
FIG. 4 (color online). (a) Close-up of a Coulomb diamond measurement around the electron-hole crossover at $B_\parallel = 0$ T. (b),(c) Cross section at $V_b = 12$ mV [white line in Fig. 3(a)] for increasing in-plane magnetic field. In (b) the traces are offset in conductivity and smoothed over a five-point window for clarity. The dashed lines in (c) have two different slopes corresponding to a Zeeman spin splitting with $g = 2$ and are plotted for comparison over the raw data.

Next we describe an attempt to observe the Zeeman splitting of excited states in parallel magnetic field. Figure 4(a) shows part of a Coulomb-blockade diamond measurement at $B = 0$ T [this is a close-up of Fig. 2(b) in Ref. [16]]. As in Fig. 1(b), several differential conductance peaks are visible. Along the white bar at $V_b = 12$ mV, the evolution of the peaks is measured in Fig. 4(c). Individual cross sections are plotted in Fig. 4(b) showing the change in amplitude and the movement of the peaks. The six peaks labeled in Fig. 4(c) are linked to the stronger resonances in Fig. 4(a). The magnetic field dependence of the two faint lines between resonances 2 and 5 in Fig. 4(a) could not be traced in Fig. 4(c). The evolution of the peaks can be attributed to two different slopes. For comparison, black dashed lines with slopes differing by the Zeeman energy $\Delta E^Z = |g|\mu_B B$ with $g = 2$ are plotted on top. Despite a slight underestimation of the splitting, the lines agree reasonably well with the measurement. Hence we attribute the two slopes to Zeeman spin splitting. The absence of clear peak splittings that would be induced by lifting the spin degeneracy with B can be seen as another indication of significant charge carrier interactions.

In summary, we have analyzed a graphene quantum dot in an in-plane magnetic field by investigating the conductance peak spacing and the evolution of excited states around the electron-hole crossover. In both regimes A and B, spin pairs were identified showing a linear and $|g| = 2$ compatible Zeeman splitting with magnetic field, whereas other conductance peaks follow a different behavior similar to observations in GaAs quantum dots [19,20]. The observed spin sequence with spin polarization and the absence

of clear degenerate ground and excited states are in agreement with the strength of Coulomb interactions expected from a comparison of interaction and kinetic energy of charge carriers in graphene. In contrast to GaAs quantum dots, we do not expect a significant dependence of the exchange interaction on the carrier density (see Refs. [19,26]), making it especially interesting to study the low carrier regime in more detail in future experiments.

*guettinj@phys.ethz.ch
†Present address: JARA-FIT and II. Institute of Physics, RWTH Aachen, 52074 Aachen, Germany.

[1] D. Loss and D. P. DiVincenzo, Phys. Rev. A **57**, 120 (1998).
[2] J. M. Elzerman et al., Nature (London) **430**, 431 (2004).
[3] J. R. Petta et al., Science **309**, 2180 (2005).
[4] B. Trauzettel, D. V. Bulaev, D. Loss, and G. Burkard, Nature Phys. **3**, 192 (2007).
[5] C. L. Kane and E. J. Mele, Phys. Rev. Lett. **95**, 226801 (2005).
[6] H. Min et al., Phys. Rev. B **74**, 165310 (2006).
[7] D. Huertas-Hernando, F. Guinea, and A. Brataas, Phys. Rev. B **74**, 155426 (2006).
[8] C. Stampfer et al., Appl. Phys. Lett. **92**, 012102 (2008); Nano Lett. **8**, 2378 (2008).
[9] L. A. Ponomarenko et al., Science **320**, 356 (2008).
[10] X. Liu et al., Phys. Rev. B **80**, 121407(R) (2009).
[11] S. Schnez et al., Appl. Phys. Lett. **94**, 012107 (2009).
[12] J. Moser and A. Bachtold, Appl. Phys. Lett. **95**, 173506 (2009).
[13] M. B. Lundeberg and J. A. Folk, Nature Phys. **5**, 894 (2009).
[14] J. Güttinger, C. Stampfer, T. Frey, T. Ihn, and K. Ensslin, Phys. Status Solidi **246**, 2553 (2009).
[15] C. Stampfer et al., Phys. Rev. Lett. **102**, 056403 (2009).
[16] J. Güttinger et al., Phys. Rev. Lett. **103**, 046810 (2009).
[17] F. Libisch et al., Phys. Rev. B **81**, 245411 (2010).
[18] S. Tarucha et al., Phys. Rev. Lett. **77**, 3613 (1996).
[19] S. Lindemann et al., Phys. Rev. B **66**, 195314 (2002).
[20] J. A. Folk et al., Phys. Scr. **T90**, 26 (2001).
[21] M. R. Buitelaar, A. Bachtold, T. Nussbaumer, M. Iqbal, and C. Schönenberger, Phys. Rev. Lett. **88**, 156801 (2002).
[22] D. H. Cobden and J. Nygard, Phys. Rev. Lett. **89**, 046803 (2002).
[23] P. Jarillo-Herrero et al., Nature (London) **429**, 389 (2004).
[24] S. Moriyama et al., Phys. Rev. Lett. **94**, 186806 (2005).
[25] T. Heinzel, Mesoscopic Electronics in Solid State Nanostructures (Wiley-Vch, Weinheim, 2003), p. 145.
[26] S. Lüscher et al., Phys. Rev. Lett. **86**, 2118 (2001).
[27] S. R. Patel et al., Phys. Rev. Lett. **80**, 4522 (1998).
[28] Y. M. Blanter, A. D. Mirlin, and B. A. Muzykantskii, Phys. Rev. Lett. **78**, 2449 (1997).